JOURNAL OF COMPUTATIONAL PHYSICS 102, 252–264 (1992)

Computation of the Direct Scattering Transform for the Nonlinear Schroedinger Equation

G. BOFFETTA AND A. R. OSBORNE

Istituto di Fisica Generale dell'Università and Istituto di Cosmo-Geofisica del C.N.R., Via Pietro Giuria 1, Turin 10125, Italy

Received October 16, 1990; revised October 17, 1991

The cubic nonlinear Schroedinger equation (NLS) describes the space–time evolution of narrow-banded wave trains in one space and one time (1 + 1) dimensions. The richness of nonlinear wave motions described by NLS is exemplified by the fully nonlinear envelope soliton and "breather" solutions, which are fully understood only in terms of the general solution of the equation as described by the inverse scattering transform (IST); the method may be viewed as a nonlinear generalization of the linear Fourier transform. Herein we develop a numerical algorithm for determining the scattering transform spectrum of a nonlinear wave train described by the NLS equation. The analysis of space or time series data obtained from computer simulations of nonlinear, narrow-band wave trains or from experimental measurements is thus a central point of discussion. In particular we develop a numerical algorithm for computing the *direct scattering transform* (DST) which may be interpreted as the nonlinear Fourier spectrum of the complex envelope function of a wave train; the fact that the nonlinear Fourier modes are constants of the motion for all time provides a physical basis for the analysis of data. While the nonlinear Fourier method is specifically applied to the NLS equation, the approach is easily generalized to include the class of spectral problems due to Ablowitz, Kaup, Newell, and Segur (AKNS). This class includes several other nonlinear wave equations of physical interest in (1 + 1), including the Korteweg–de Vries (KdV), modified KdV, sine-Gordon, and sinh-Gordon equations. © 1992 Academic Press, Inc.

1. INTRODUCTION

The theoretical study of nonlinear wave motion was revolutionized by the discovery of the *inverse scattering transform* by Martin Kruskal and co-workers more than 20 years ago (GGKM) [1]. This new method of mathematical physics was inspired by the important computer experiments of Zabusky and Kruskal [2] who studied numerical solutions of the Korteweg–de Vries (KdV) equation. The GGKM scattering transform provides the *general solution* to the KdV equation for *asymptotic, infinite-line boundary conditions*. The approach is a generalization of ordinary Fourier analysis to nonlinear problems and has been extended to a large class of physically relevant nonlinear wave equations by Zakharov and Shabat [3], and Ablowitz, Kaup, Newell, and Segur (AKNS) [4]. Among the integrable equations in this class are the KdV, modified KdV, nonlinear Schroedinger (NLS), sine-Gordon, and sinh-Gordon equations.

Soon after the discovery of the spectral solution to KdV on the infinite line, Dubrovin, Matveev, and Novikov [5, 6] found the solution to KdV for *periodic boundary conditions*, and consequently discovered how to generalize the scattering transform to *nonlinear Fourier series*. Periodic IST was subsequently extended to other nonlinear wave equations such as NLS, sine-Gordon, and sinh-Gordon equations [7–11].

Because the Fourier transform and Fourier series have long been important tools in the analysis of wave data, it is perhaps surprising that IST has not been used more extensively for the analysis of *nonlinear* data. There are evidently two reasons why this has not occurred. One is the mathematical complexity of the scattering transform, particularly for periodic boundary conditions. Consequently the physical interpretation of this mathematical machinery has not been easily transparent and readily amenable to the analysis of data. The second difficulty is that reliable numerical methods have not been available for efficiently using IST in an experimental context.

Up to the present time numerical methods have been available only for the KdV, NLS, and sine-Gordon equations. Results for the KdV equation have been documented in a series of papers by Osborne and co-workers [12–23]. Numerical procedures for the sine-Gordon equation (and the NLS equation in a certain limit of sine-Gordon) have also been developed [11, 24]; a sixth-order numerical integrator was used to obtain solutions to the spectral eigenvalue problem. A discrete version of the inverse scattering transform for the AKNS class of spectral problems on the infinite line has been developed by Ablowitz and Ladik [25, 26].

In the present paper we focus on numerical methods for determining the nonlinear spectral structure of wave motion described by the NLS equation for infinite-line boundary

0021-9991/92 $5.00
Copyright © 1992 by Academic Press, Inc.
All rights of reproduction in any form reserved.

conditions. NLS was first derived by Zakharov [27], who together with Shabat [3] found the inverse scattering transform solution to NLS on the infinite line. Physical motivation for the study of the NLS equation stems from the important work of Yuen and Lake [28–31] who verified in laboratory experiments the existence of envelope solitons, which remarkably resemble the soliton solutions to the NLS equation. These solutions arise asymptotically in time from an initial, narrow-banded wave train (see Fig. 1).

In the present study we focus on and extend an approach for numerically determining the scattering transform of NLS as recently developed by Osborne [22] for the KdV equation (see also [23]). The procedure for NLS is illustrated in Fig. 2. A dynamically evolving nonlinear, narrow-banded wave train (Fig. 2a) is assumed to have a complex envelope $q(x, t) = A(x, t)\exp(i\phi(x, t))$, for $A(x, t)$ the real envelope and $\phi(x, t)$ the real phase. The envelope $q(x, t)$ is assumed to be computable from the wave train by (say) the Hilbert transform. The wave train is numerically sampled at discrete intervals Δx and the discrete Hilbert transform is then used to generate a discrete envelope function as shown in Fig. 2b. The discrete envelope is subsequently replaced by a piecewise constant function whose "partitions" are centered around the discrete points (Fig. 2c). The numerical scattering transform algorithm developed here is analytically exact for this piecewise constant envelope function.

It is important in what follows to understand that we are *not* presenting an approach to numerically integrate the NLS equation in order to obtain its space–time solution,

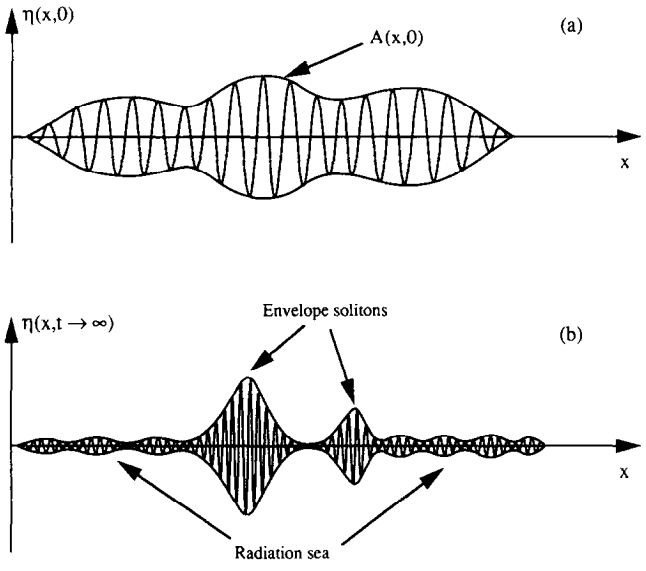

FIG. 1. (a) A narrow-banded wave train at time $t = 0$ evolves into envelope solitons and a background sea of radiation as $t \to \infty$ (b). Note that we have taken the spatial scale in (b) to be much greater than in (a) to include the entire wave train after it has been substantially spatially dispersed.

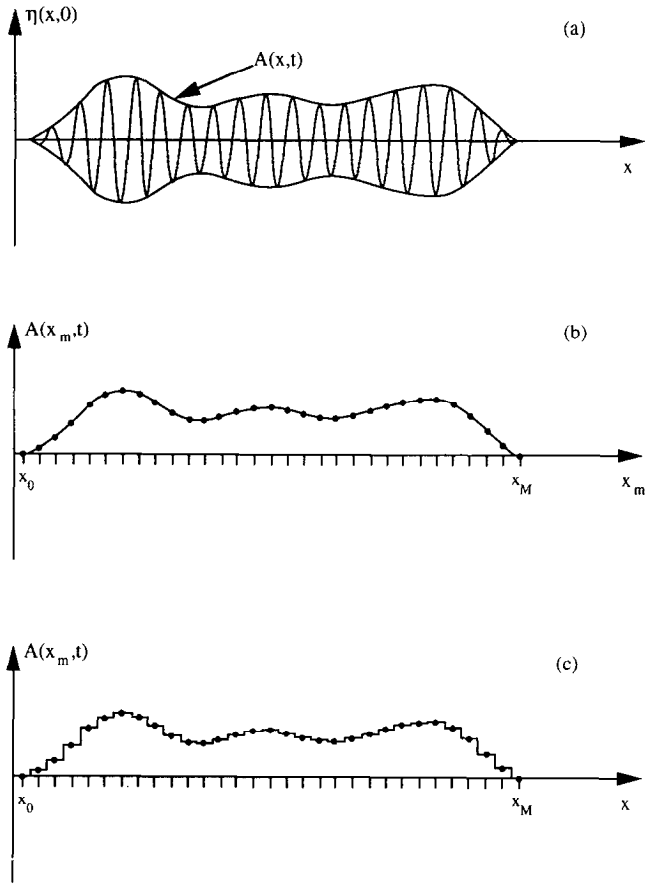

FIG. 2. (a) A narrow-banded nonlinear wave train $\eta(x, 0)$ with complex envelope $q(x, 0) = A(x, 0)\exp[i\phi(x, 0)]$ is assumed given as a function of x at time $t = 0$. Note that the wave train is localized on the interval $-\infty < x < \infty$, i.e., $A(x, 0) \to 0$ as $|x| \to \infty$. The wave train of (a) is discretized at intervals Δx and, with the aid of the Hilbert transform, the discrete envelope function $A(x_n, 0)$ is computed (b). In order to determine the scattering transform the discrete envelope in (b) is replaced by a piecewise constant function (c). The direct scattering transform algorithm given herein is analytically exact for wave envelopes of this type.

$q(x, t)$, given a particular initial condition $q(x, 0)$. There is already a marvelous, vast literature on standard techniques for numerical integrations of this type, which include split-step Fourier methods, modal decomposition, and finite-differencing. What we are instead doing herein is *developing methods for determining the spectral structure* of $q(x, t_0)$ (t_0 is some arbitrary fixed value of time), based upon the *inverse scattering transform.* Since IST is a kind of nonlinear Fourier analysis, we are therefore *developing methods for the nonlinear Fourier analysis of space series* (and, as we discuss elsewhere, also of time series [15, 17]). We foresee a number of applications of our approach, including (1) the space and time series analysis of experimental data, (2) the space and time series analysis of computer generated signals, (3) the checkout of numerical algorithms (such as those mentioned above for the space–time integration of the NLS equation), and (4) the search for "chaotic effects"

in NLS. All of these applications present the possibility of uncovering new physics in a wide variety of problems.

The analysis of data using the scattering transform is becoming increasingly sophisticated [19–21] and a number of studies are now under way in the other areas. These include the interesting area of research in which certain "chaotically appearing solutions" to the nonlinear Schroedinger equation appear. Despite intensive studies, the behavior of solutions of the nonlinear Schroedinger equation is far from settled. Recent numerical experiments (see [30, 31] for reviews) indicate (a) that certain solutions to NLS appear "choatic" even though the equation is known to be completely integrable and (b) that the degree of "chaos" decreases with the addition of high frequency modes. We feel that application of the inverse scattering approach to this intriguing problem may lead to important physical insight. The study of this problem, however, requires periodic boundary conditions, which are beyond the scope of this paper. In forthcoming papers we deal with both periodic boundary conditions and the search for "chaos" in NLS.

The rest of the paper is organized as follows. In Section 2 we discuss the physics of wave propagation as described by NLS and in Section 3 we give an overview of the associated inverse scattering transform. Section 4 discusses the numerical approach for determining the direct scattering transform spectrum, while Section 5 relates this method to previous approaches. Numerical tests of the algorithm are given in Section 6.

2. THE NONLINEAR SCHROEDINGER EQUATION

The NLS equation describes the space–time evolution of nonlinear, narrow-banded, small amplitude wave trains in one space and one time dimensions $(1+1)$ (Fig. 1). In standard dimensionless form NLS is written as

$$iq_t - q_{xx} + 2\sigma |q|^2 q = 0. \tag{2.1}$$

Depending upon the sign $\sigma\ (=\pm 1)$ of the nonlinear term in this equation the motion is dominated primarily by either "shallow" or "deep water" wave physics. The deep water (or focusing, $\sigma = -1$) case is known to have envelope solitons and "breather" solutions, results which have fueled recent conjectures about the possibility of coherent propagating wave packets in oceanic surface and internal wave motions [28–31]. In the shallow (or defocusing, $\sigma = +1$) case, where envelope soliton solutions cannot occur, the motion is nevertheless still quite rich and is similar to wave propagation described by the Korteweg–de Vries (KdV) equation [16, 17, 20, 32].

The history of the nonlinear Schroedinger equation dates back to 1847, when Stokes [33] determined an amplitude-dependent correction to the linear dispersion relation for surface water waves. More than a century later NLS was derived by Zakharov [27] and Hasimoto and Ono [34]; the amplitude-dependent correction found by Stokes determines the nonlinear behavior of this equation. The NLS equation has since been obtained in a wide variety of physical contexts from a large number of primitive nonintegrable PDEs [35]. For example, NLS has been derived in the context of water waves, plasma physics, and nonlinear optics [36–40].

Generally speaking, NLS is derived from primitive PDEs by focusing on the slow space–time modulation of a quasi-monochromatic wave packet. NLS may also be derived from the KdV equation using the multiscale technique [16, 17, 20, 32, and references cited therein]. The major advantage of this latter approach is that it gives the specific mathematical relationship between the scattering transform spectra for (defocusing) NLS and KdV for both infinite-line [41] and periodic boundary conditions [16, 17, 20, 32].

A simple, heuristic derivation of NLS helps to explain why it is a generic equation [7]. Let $\Theta(x, t)$ describe a narrow-banded complex wave field (the real wave amplitude is then defined by $\eta(x, t) = \mathrm{Re}(\Theta(x, t))$), propagating in a dispersive medium in which the dispersion relation depends upon the modulus, $\omega = \omega(k, |\Theta|^2)$. The Fourier representation of $\Theta(x, t)$ is:

$$\Theta(x, t) = \int_{-\infty}^{+\infty} F(k)\, e^{i(kx - \omega t)}\, dk. \tag{2.2}$$

For (2.2) to describe narrow-banded, nonlinear wave motion, $F(k)$ must be sharply peaked around some k_0 (monochromatic wave propagation). We therefore expand ω in a Taylor series around $k = k_0$ and $|\Theta|^2 = 0$. To leading order we obtain

$$\Theta(x, t) = e^{i(k_0 x - \omega_0 t)} \int_{-\infty}^{+\infty} F(\kappa) \times \exp\left[i\kappa x - i\left(\kappa\omega_0' + \frac{\kappa^2}{2}\omega_0'' + \alpha |\Theta|^2 \right) t \right] d\kappa, \tag{2.3}$$

where $\kappa = k - k_0$, $\omega_0 = \omega(k_0, 0)$, and the prime denotes the derivative with respect to k. Here α is a constant which depends on the physics of the problem at hand. For example, surface water waves in shallow water have the dispersion relation $\omega = c_0 k - \beta k^3 + \alpha |\Theta|^2$ for $c_0 = \sqrt{gh}$, $\beta = c_0 h^2/6$, and $\alpha = -9c_0/16k_0 h^4$ [19, 34]. If we set $\Theta(x, t) = q(x, t)\, e^{i(k_0 x - \omega_0 t)}$, where $e^{i(k_0 x - \omega_0 t)}$ denotes the carrier wave, and then taking the spatial and temporal derivatives of (2.3) we obtain

$$i(q_t + \omega_0' q_x) + \tfrac{1}{2}\omega_0'' q_{xx} - \alpha |q|^2 q = 0 \tag{2.4}$$

which can be put in the dimensionless form (2.1) by means of the transformation

$$\begin{aligned} q &\to \sqrt{(|\alpha|/2)}\, q \\ x &\to \sqrt{-(2/\omega_0'')}\,(x-\omega_0' t) \\ \sigma &= \operatorname{sgn}(-\alpha). \end{aligned} \tag{2.5}$$

The sign $\sigma = \pm 1$ distinguishes between the "stable" and "unstable" forms of NLS. The stable, or defocusing, case arises when $\sigma = +1$ for which there are no soliton solutions. In this case the wave motion behaves much like the KdV equation in the narrow-banded approximation [16, 17, 20, 32]. When $\sigma = -1$ the NLS equation lies in the "focusing" regime and is linearly unstable to modulational perturbations; the initial condition $q(x, 0)$ generally evolves over time into one or more solitons and radiation (see Fig. 1). Fermi–Pasta–Ulam recurrence prevails in the periodic problem [28–31].

In this paper we develop a numerical algorithm for the direct spectral problem of the NLS equation on the infinite line. Infinite-line boundary conditions require (for NLS to have a well-behaved solution) that $q(x, t)$ decay sufficiently fast so that as $|x| \to \infty$, the Gelfand–Levitan–Marchenko integral equation solves NLS (see Section 3 below and [35] for details).

The soliton solution to NLS (which occurs in the case $\sigma = -1$) can be written as the complex function

$$q(x, t) = q_0 e^{-i(kx-\omega t)} \operatorname{sech}(px - rt), \tag{2.6}$$

where $p^2 = |q_0|^2$, $\omega = k^2 - p^2$, and $r = 2pk$. Solutions of this type have the remarkable property that they are preserved upon collision with each other, e.g., the interaction, while being quite nonlinear, is characterized by the fact that the solitons retain their shapes and speeds after the collision, but are phase shifted relative to their positions in the absence of the collision. In addition to (2.6) we also employ the N-soliton solution to the NLS equation for numerical checkout purposes [35, 42].

3. THE INVERSE SCATTERING TRANSFORM FOR NLS

IST can be thought of as a generalization of the linear Fourier transform (which solves linear partial differential equations) but, unlike that method, IST works only for specific classes of equations which are normally referred to as being "integrable." The integrability implies the existence of an infinite number of conservation laws, the first few of which are the conservation of mass, momentum, and energy.

The spectral problem for NLS is formulated as an eigenvalue problem for an auxiliary spectral function ψ, in which the complex envelope $q(x, t)$, the solution to NLS (2.1), acts as a "potential." One shows that if q is a solution to NLS, the eigenvalue problem is isospectral; i.e., the soliton eigenvalues do not change in time. One can then solve the linear eigenvalue problem for a certain time (say t_0) to find the scattering transform spectrum (defined below in (3.8), (3.9)). The time dependencies of the spectrum are simple (Fourier-like, (3.10) below) and one can evaluate the spectrum for any other time (say t_1). This last step is the inverse problem and consists of solving a linear integral equation due to Gelfand, Levitan, and Marchenko (GLM, (3.11) below) [4].

The eigenvalue or spectral problem for NLS is [35]

$$\Psi_x = Q(\zeta)\,\Psi, \qquad Q = \begin{pmatrix} -i\zeta & q \\ \sigma q^* & -i\zeta \end{pmatrix}, \tag{3.1}$$

where ζ is the (time-independent) complex spectral wavenumber. Given a suitable linear time evolution for the complex spectral field $\Psi(x, \zeta) = (\psi_1, \psi_2)$, one obtains from the compatibility condition $\Psi_{tx} = \Psi_{xt}$ the PDE for the potential $q(x, t)$ (2.1) [35].

It is easily shown that if Ψ is a solution to (3.1), another linearly independent solution is given by $\bar{\Psi}(x, \zeta)$

$$\bar{\Psi}(x, \zeta) = c \begin{pmatrix} 0 & \sigma \\ 1 & 0 \end{pmatrix} \Psi^*(x, \zeta^*) = \begin{pmatrix} c\sigma\psi_2^*(\zeta^*) \\ c\psi_1^*(\zeta^*) \end{pmatrix} \tag{3.2}$$

for c an arbitrary constant. Following Ref. [35] we choose two solutions which have the following asymptotic behaviour

$$\begin{aligned} \Psi(x, \zeta) &\to \begin{pmatrix} 1 \\ 0 \end{pmatrix} e^{-i\zeta x} \qquad \text{as} \quad x \to \infty \\ \Phi(\zeta, x) &\to \begin{pmatrix} 1 \\ 0 \end{pmatrix} e^{-i\zeta x} \qquad \text{as} \quad x \to -\infty \end{aligned} \tag{3.3}$$

For associated solutions $\bar{\Psi}$ and $\bar{\Phi}$ we choose respectively $c = 1$ and $c = -1$ for which

$$\begin{aligned} \bar{\Psi}(x, \zeta) &= \begin{pmatrix} \sigma\psi_2^*(\zeta^*) \\ \psi_1^*(\zeta^*) \end{pmatrix} \to \begin{pmatrix} 0 \\ 1 \end{pmatrix} e^{i\zeta x}, \qquad \text{as} \quad x \to \infty \\ \bar{\Phi}(x, \zeta) &= -\begin{pmatrix} \sigma\phi_2^*(\zeta^*) \\ \phi_1^*(\zeta^*) \end{pmatrix} \to -\begin{pmatrix} 0 \\ 1 \end{pmatrix} e^{i\zeta x}, \qquad \text{as} \quad x \to -\infty. \end{aligned} \tag{3.4}$$

We then use the definition of the Wronskian, $W(u, v) = u_1 v_2 - u_2 v_1$, which has the property $\partial W/\partial x = 0$, and show that $W(\Psi, \bar{\Psi}) = 1$ and $W(\Phi, \bar{\Phi}) = -1$. The scattering coefficients are then defined by the expansions

$$\begin{aligned} \Phi(x, \zeta) &= a(\zeta)\,\Psi(x, \zeta) + b(\zeta)\,\bar{\Psi}(x, \zeta) \\ \bar{\Phi}(x, \zeta) &= \bar{b}(\zeta)\,\Psi(x, \zeta) - \bar{a}(\zeta)\,\bar{\Psi}(x, \zeta). \end{aligned} \tag{3.5}$$

In the limit as $x \to \infty$ we obtain from (3.5):

$$\begin{aligned} a(\zeta) &= \lim_{x\to\infty} \phi_1(x,\zeta)\, e^{i\zeta x} \\ b(\zeta) &= \lim_{x\to\infty} \phi_2(x,\zeta)\, e^{-i\zeta x} \\ \bar{a}(\zeta) &= -\lim_{x\to\infty} \phi_2'(x,\zeta)\, e^{-i\zeta x} = a^*(\zeta^*) \\ \bar{b}(\zeta) &= \lim_{x\to\infty} \phi_1'(x,\zeta)\, e^{i\zeta x} = -\sigma b^*(\zeta^*). \end{aligned} \tag{3.6}$$

The transmission coefficient $a(\zeta)$ and reflection coefficient $b(\zeta)$ then satisfy:

$$a(\zeta)\, a^*(\zeta^*) - \sigma b(\zeta)\, b^*(\zeta^*) = 1. \tag{3.7}$$

When $\sigma = -1$, the scattering problem (3.1) can have bound states (envelope solitons); these occur whenever $a(\zeta)$ has a zero in the upper half plane, $\mathrm{Im}(\zeta) > 0$ (and Φ is proportional to $\bar{\Psi}$). These zeros correspond to soliton solutions, e.g., nondispersive localized wave packets that collide elastically [4, 35]. We denote the N zeros of $a(\zeta)$ (soliton eigenvalues) by ζ_k.

When $\sigma = +1$ the eigenvalue problem (3.1) is hermitian and there are no eigenvalues with $\mathrm{Im}(\zeta) > 0$. In this case no envelope soliton solutions are possible.

The scattering spectrum for a complex envelope $q(x, t=0)$, is defined by:

Discrete (soliton) spectrum,

$$\begin{aligned} &N \text{ eigenvalues } \zeta_k \in \mathbf{C} \text{ for which } a(\zeta_k) = 0 \\ &N \text{ phase coefficients } \rho_k = \left(\frac{b(\zeta)}{a'(\zeta)}\right)_{\zeta=\zeta_k} \\ &\qquad\qquad (a'(\zeta) = \partial a/\partial\zeta). \end{aligned} \tag{3.8}$$

Continuous (radiation) spectrum,

$$\rho(\xi) = \frac{b(\xi)}{a(\xi)}, \qquad \xi \in \mathbf{R}. \tag{3.9}$$

Note that the discrete eigenvalues lie in the complex plane, while the continuous spectrum lies on the real axis. Given the quantities (3.8) and (3.9), one can reconstruct the potential field $q(x, 0)$ by solving the GLM equation [4]. This reconstruction can conveniently be done at any value of time to determine $q(x, t)$. One first determines the coefficients $a(\zeta)$, $b(\zeta)$ at some arbitrary time t by:

$$\begin{aligned} a(\zeta, t) &= a(\zeta, 0) \\ b(\zeta, t) &= b(\zeta, 0) \exp(-4i\zeta^2 t)). \end{aligned} \tag{3.10a}$$

Thus $a(\zeta, t)$ is time independent while $b(\zeta, t)$ varies sinusoidally. The temporally varying scattering transform spectrum is then:

$$\begin{aligned} \zeta_k(t) &= \zeta_k \\ \rho_k(t) &= \left(\frac{b(\zeta, t)}{a'(\zeta)}\right)_{\zeta=\zeta_k} \\ \rho(\xi) &= \frac{b(\xi, t)}{a(\xi)}. \end{aligned} \tag{3.10b}$$

The temporal evolution of the envelope $q(x, t)$ is governed by the Fourier-like relations (3.10a), as we now see. The inverse scattering transform is the solution to the GLM equation

$$K(x, y) + \sigma F^*(x+y) + \sigma \int_x^\infty ds \int_x^\infty dr\, K(x, r)\, F(r+s)\, F^*(s+y) = 0. \tag{3.11}$$

Here the kernel $F(x)$ is given in terms of the spectrum

$$F(x) = \frac{1}{2\pi}\int_{-\infty}^{\infty} \rho(\xi, t)\, e^{i\xi x}\, d\xi - i \sum_{k=1}^{N} \rho_k(t)\, e^{i\zeta k x} \tag{3.12}$$

and the potential field (the solution to the KdV equation) is reconstructed (at time t) by the formula

$$q(x, t) = -2K(x, x; t). \tag{3.13}$$

In summary the direct scattering transform consists of computing the spectrum (3.8), (3.9). Time evolution of the spectrum is determined by (3.10). The inverse scattering transform generates the spatial-temporal solution to NLS (3.11)–(3.13). Note that time, which plays the role of a parameter in the inverse problem, has been suppressed in (3.11).

Conservation laws for the NLS equation are found by an asymptotic expansion of the field Ψ in inverse powers of ζ [3]. This method gives the infinite number of conserved quantities both in terms of the field $q(x, t)$ and in terms of the scattering data. The first of these quantities is the mass:

$$\begin{aligned} C_0 &= -\sigma \int_{-\infty}^{+\infty} |q(x, t)|^2\, dx \\ &= -\frac{1}{\pi}\int_{-\infty}^{+\infty} \ln |a(\xi)|^2\, d\xi + \sum_{k=1}^{N} 2i(\zeta_k^* - \zeta_k). \end{aligned} \tag{3.14}$$

This equation, a generalization of the Parseval relation for the Fourier transform, is useful in the numerical implementation of the DST, as discussed below. The time evolution of

the scattering spectrum (3.10) emphasizes the deep similitude between the DST and the Fourier transform.

We now show explicitly that for a "small-amplitude" envelope $q(x, 0)$, the scattering transform spectrum tends to the Fourier spectrum [4]. Let the complex envelope be of order ε, $q(x, 0) \to \varepsilon q(x, 0)$, for ε small. The direct scattering problem becomes

$$\begin{aligned} \psi_{1x} - \varepsilon q \psi_2 + i\zeta \psi_1 &= 0 \\ \psi_{2x} - \varepsilon \sigma q^* \psi_1 - i\zeta \psi_2 &= 0. \end{aligned} \tag{3.15}$$

A solution with the asymptotic behavior of Φ (3.3)–(3.4) is then of the form,

$$\begin{aligned} \phi_1(x) &= e^{-i\zeta x}\left(1 + \varepsilon \int_{-\infty}^{x} q(x, 0)\, e^{2i\zeta x}\, dx\right) \\ \phi_2(x) &= e^{i\zeta x} \varepsilon \int_{-\infty}^{x} \sigma q^*(x, 0)\, e^{-2i\zeta x}\, dx, \end{aligned} \tag{3.16}$$

to leading order in ε, so that from (3.6) we find

$$\begin{aligned} a(\zeta) &= 1 + \varepsilon \int_{-\infty}^{+\infty} q(x, 0)\, e^{2i\zeta x}\, dx \\ b(\zeta) &= \varepsilon \int_{-\infty}^{+\infty} \sigma q^*(x, 0)\, e^{-2i\zeta x}\, dx. \end{aligned} \tag{3.17}$$

Using the definition of the Fourier transform,

$$F[u(x), k] = \frac{1}{\sqrt{2\pi}} \int_{-\infty}^{+\infty} u(x)\, e^{-ikx}\, dx, \tag{3.18}$$

we see that for real $\zeta = \xi$,

$$\begin{aligned} a(\zeta) &= 1 + \varepsilon \sqrt{2\pi}\, F[q(x, 0); -2\xi] \\ b(\zeta) &= \varepsilon \sqrt{2\pi}\, \sigma F^*[q(x, 0); -2\xi] \end{aligned} \tag{3.19}$$

and then, by (3.9), at leading order,

$$\rho(\xi) = \varepsilon \sqrt{2\pi}\, \sigma F^*[q(x, 0); -2\xi]. \tag{3.20}$$

This latter result may be understood best by linearizing (3.11),

$$q(x, 0) = -2K(x, x) = 2\sigma F^*(2x), \tag{3.21}$$

and remembering that, for a "small" potential (of order ε) there are no discrete eigenvalues, so from (3.12),

$$q(x, 0) = \frac{\sigma}{\pi} \int_{-\infty}^{+\infty} \rho^*(\xi)\, e^{-2i\xi x}\, d\xi. \tag{3.22}$$

Thus (3.20), together with (3.22), shows that the continuous spectrum $\rho(\xi)$ (3.9) reduces to the ordinary Fourier transform in the linear limit of the wave motion. Note, further, that in the linear limit relation, (3.14) reduces exactly to the Parseval equation:

$$\int_{-\infty}^{+\infty} |q(x, 0)|^2\, dx = \int_{-\infty}^{+\infty} |F(q, \xi)|^2\, d\xi. \tag{3.21}$$

4. A NUMERICAL METHOD FOR THE DIRECT SCATTERING TRANSFORM

We now develop a numerical algorithm for the direct scattering transform in wavenumber space. The algorithm uses a discretization of the complex wave envelope $q(x, 0)$ in $2M + 1$ steps of constant values q_n at points $x_n = n\, \Delta x$ with spatial interval $\Delta x = L/M$ (where $2L$ is the width of the wave train centered on $x = 0$, i.e., $q(x, 0) = 0$ for $|x| \geqslant L$; see Fig. 2). The solution of the spectral eigenfunction Ψ in each interval Δx is then obtained by direct integration of (3.1),

$$\Psi(x_n + \Delta x) = U(q_n)\, \Psi(x_n), \tag{4.1}$$

where $U(q, \Delta x)$ is the exponential of the *trace-vanishing* matrix $Q(\zeta)$ (3.1),

$$\begin{aligned} U(q) &= \exp[\Delta x Q(\zeta)] = \exp\left(\Delta x \begin{pmatrix} -i\zeta & q \\ \sigma q^* & i\zeta \end{pmatrix}\right) \\ &= \begin{pmatrix} \cosh(k\,\Delta x) - \dfrac{i\zeta}{k} \sinh(k\,\Delta x) & \dfrac{q}{k} \sinh(k\,\Delta x) \\ \dfrac{\sigma q^*}{k} \sinh(k\,\Delta x) & \cosh(k\,\Delta x) + \dfrac{i\zeta}{k} \sinh(k\,\Delta x) \end{pmatrix} \end{aligned} \tag{4.2}$$

and $k^2 = \sigma |q|^2 - \zeta^2$ is constant inside an interval Δx. Therefore, we have used a standard exponential propagator method to solve the scattering problem (3.1) when $q(x, 0)$ is constant in the interval Δx [43].

We now introduce a four-component field consisting of Ψ and its derivative with respect to ζ,

$$\Xi(x, \zeta) = \begin{pmatrix} \Psi \\ \Psi' \end{pmatrix}, \tag{4.3}$$

where $\Psi' = \partial \Psi / \partial \zeta$. For the field Ξ we have a recursion relation given in terms of (4.2) by

$$\Xi(x_n + \Delta x) = T(q_n)\, \Xi(x_n), \tag{4.4a}$$

where

$$T(q_n) = \begin{pmatrix} U(q_n) & 0 \\ U'(q_n) & U(q_n) \end{pmatrix} \tag{4.4b}$$

is a four-by-four matrix and $U'(q_n) = \partial U(q_n)/\partial\zeta$ is given by

$$
\begin{aligned}
U'_{11} &= i\,\Delta x \frac{\zeta^2}{k^2}\cosh(k\,\Delta x) - \left(\zeta\,\Delta x + i + i\frac{\zeta^2}{k^2}\right)\frac{\sinh(k\,\Delta x)}{k} \\
U'_{12} &= -\frac{q\zeta}{k^2}\left(\Delta x\cosh(k\,\Delta x) - \frac{\sinh(k\,\Delta x)}{k}\right) \\
U'_{21} &= -\frac{\sigma q^*\zeta}{k^2}\left(\Delta x\cosh(k\,\Delta x) - \frac{\sinh(k\,\Delta x)}{k}\right) \\
U'_{22} &= -i\,\Delta x \frac{\zeta^2}{k^2}\cosh(k\,\Delta x) - \left(\zeta\,\Delta x - i - i\frac{\zeta^2}{k^2}\right)\frac{\sinh(k\,\Delta x)}{k}.
\end{aligned}
\tag{4.5}
$$

The discretization of $q(x, 0)$ in $2M+1$ constant steps,

$$
q(x,0) = q_n \qquad \text{for} \quad x \in \left(x_n - \frac{\Delta x}{2}; x_n + \frac{\Delta x}{2}\right], \tag{4.6}
$$

allows us to write the (discrete) solution to the scattering problem as

$$
\Xi(x_n) = \prod_{j=n-1}^{-M} T(q_j)\,\Xi(x_{-M}). \tag{4.7}
$$

The scattering coefficients can now be obtained from relations (3.5) in terms of a *scattering matrix* S which is written in terms of the submatrix Σ and its derivative $\Sigma' = \partial\Sigma/\partial\zeta$,

$$
S(\zeta) = \prod_{j=M-1}^{-M} T(q_j) = \begin{pmatrix} \Sigma(\zeta) & 0 \\ \Sigma'(\zeta) & \Sigma(\zeta) \end{pmatrix}, \tag{4.8}
$$

where

$$
\Sigma = \prod_{j=M-1}^{-M} U(q_j). \tag{4.9}
$$

Formally speaking, the matrix $S(\zeta)$ carries solutions of the eigenvalue problem (3.1) from $-\infty$ to $+\infty$; numerically, $S(\zeta)$ carries solutions (4.3) of (3.1) from $-L$ to L. We write this result

$$
\begin{pmatrix} \Psi(L,\zeta) \\ \Psi'(L,\zeta) \end{pmatrix} = \begin{pmatrix} \Sigma(\zeta) & 0 \\ \Sigma'(\zeta) & \Sigma(\zeta) \end{pmatrix} \begin{pmatrix} \Psi(-L,\zeta) \\ \Psi'(-L,\zeta) \end{pmatrix}, \tag{4.10}
$$

where from (3.3)–(3.5) we know that

$$
\begin{aligned}
\Psi(-L,\zeta) &= \begin{pmatrix} 1 \\ 0 \end{pmatrix} e^{i\zeta L} \\
\Psi(L,\zeta) &= a(\zeta)\begin{pmatrix} 1 \\ 0 \end{pmatrix} e^{-i\zeta L} + b(\zeta)\begin{pmatrix} 0 \\ 1 \end{pmatrix} e^{i\zeta L}.
\end{aligned}
\tag{4.11}
$$

Inserting (4.11) into (4.10), we determine the scattering coefficients and their derivatives:

$$
\begin{aligned}
a(\zeta) &= S_{11}(\zeta)\, e^{2i\zeta L} \\
b(\zeta) &= S_{21}(\zeta) \\
\frac{\partial a(\zeta)}{\partial\zeta} &= [S_{31} + iL(S_{11} + S_{33})]\, e^{2i\zeta L} \\
\frac{\partial b(\zeta)}{\partial\zeta} &= S_{41} + iL(S_{43} - S_{21}).
\end{aligned}
\tag{4.12}
$$

We now briefly summarize the above numerical algorithm for determination of the scattering transform spectrum. Given a discrete complex envelope function $q_n = q(x_n, 0)$ $(-M \leqslant n \leqslant M)$, compute the $U(q_n)$ and $U'(q_n)$ matrices (4.2), (4.5) for each discrete point q_n and form the matrix $T(q_n)$ by (4.4b). The scattering matrix $S(\zeta)$ is then found by (4.8) as a product of the $2M$ $T(q_n)$ matrices (or in terms of the $\Sigma(\zeta)$ matrices (4.8), (4.9)). The transmission and reflection coefficients $a(\zeta)$, $b(\zeta)$ are computed from (4.12). The discrete soliton spectrum is then given by the solutions of (3.8) and the continuous spectrum by (3.9). To find the numerical solutions of (3.8) we implemented a standard iterative Newton method for determining the zeros of $a(\zeta_k) = 0$, where the ζ_k are complex numbers. Knowledge of the analytical form for the derivative of the scattering coefficients (4.12) makes convergence of the algorithm very fast and accurate.

Before discussing the numerical results we make some general remarks about our algorithm:

(i) Because k is given by the square root of a complex number $(k = \sqrt{\sigma\,|q|^2 - \zeta^2})$, we could be faced with an ambiguous sign convention in the complex plane; but the choice of $U(q)$ in the form (4.2) avoids this possibility because the matrix $T(q)$ is independent of the choice of the sign of k.

(ii) The matrices $T(q)$ and $U(q)$ have determinant equal to one, so that the relation (3.7) for the scattering coefficients $a(\zeta)$, $b(\zeta)$ is automatically satisfied.

(iii) In the case $\Delta x \ll 1$, the matrix $U(q)$ (4.2) reduces to

$$
U(q) \approx \begin{pmatrix} 1 - i\zeta\,\Delta x & q\,\Delta x \\ \sigma q^*\,\Delta x & 1 + i\xi\,\Delta x \end{pmatrix}. \tag{4.13}
$$

This is the form employed directly by Ablowitz and Ladik to study the discrete NLS equation [25, 26]. They derived a numerical scheme for integrating the NLS equation (as well as many other integrable equations) from the discrete scattering problem (4.13). The strength of their method is that, for certain discrete evolution equations, it is completely integrable by the inverse scattering transform. Their

approach turns out to not be very useful for the analysis of experimental data (especially for a small number of data points) because (4.13) is a discretization at first order in Δx of the associated continuous problem. In a separate study we find that the error in the numerical spectrum as computed by the method of Ablowitz and Ladik is proportional to Δx, while the approach given herein has errors proportional to $(\Delta x)^2$ [44].

(iv) The search for the discrete spectrum is conducted only in the upper half of the complex ζ plane. This is a consequence of a symmetry of the IST spectrum for the NLS equation, whose solutions are invariant for transformations of the discrete spectrum of the form $(\zeta_k, \rho_k) \to (\zeta_k^*, -\rho_k^{*-1})$ [46].

5. CONNECTION TO PREVIOUS NUMERICAL APPROACHES

It is well known that the general AKNS scattering problem [4] contains, as a particular case, the scattering problem for the KdV equation on the infinite interval. The IST for the KdV equation has been considered by Osborne [22] (see also [23]), who developed a numerical algorithm for computing the scattering transform spectrum. It is worthwhile considering how the method presented here relates to this previous approach.

The numerical algorithm described in Section 4 can be extended to the general AKNS problem simply by substituting $\sigma q^*(x)$ by a second function $r(x)$ in every formula. It is known that the scattering problem for the KdV equation is obtainable from the AKNS problem by setting $r(x) = -1$ [35]. This implies replacing σq^* in Section 4 with -1 and we obtain from (4.1)–(4.2),

$$\psi_1(n) = -\frac{k_n}{\sinh_n}\psi_2(n+1) + \left(\frac{k_n \cosh_n}{\sinh_n} + i\zeta\right)\psi_2(n) \tag{5.1a}$$

$$\frac{k_{n+1}}{\sinh_{n+1}}\psi_2(n+2) - \frac{k_{n+1}\cosh_{n+1}}{\sinh_{n+1}}\psi_2(n+1) - \frac{k_n \cosh_n}{\sinh_n}\psi_2(n+1) + \frac{k_n \cosh_n^2}{\sinh_n}\psi_2(n) - k_n^2 \sinh_n \psi_2(n) = 0, \tag{5.1b}$$

where we have used $k_n = \sqrt{-q_n - \zeta^2}$, $\cosh_n = \cosh(k_n \Delta x)$, $\sinh_n = \sinh(k_n \Delta x)$, and $\psi_i(n) = \psi_i(x_n)$. Using a two-component field Φ defined by

$$\phi_1(n) = \psi_2(n)$$
$$\phi_2(n) = \frac{k_n}{\sinh_n}\phi_1(n+1) - \frac{k_n \cosh_n}{\sinh_n}\phi_1(n) \tag{5.2}$$

and defining $p_n = ik_n$, we obtaind a one-step algorithm analogous to (4.1):

$$\begin{pmatrix}\phi_1(n+1)\\ \phi_2(n+1)\end{pmatrix} = \begin{pmatrix}\cos(p_n) & \dfrac{\sin(p_n)}{p_n}\\ -p_n \sin(p_n) & \cos(p_n)\end{pmatrix}\begin{pmatrix}\phi_1(n)\\ \phi_2(n)\end{pmatrix}. \tag{5.3}$$

This result may also be derived from the Schroedinger eigenvalue problem for the KdV equation by applying the procedure of Section 4 above [44].

The computation of the scattering coefficients given in Osborne [22] is by means of a two-point algorithm: one solves the scattering problem for the potential barrier between two points x_n and x_{n+1}, obtaining the matrix ΔT_n that connects the solution of the eigenvalues problem from x_{n+1} to x_n. The scattering coefficients are then essentially given by the product of the $2M$ matrices ΔT_n:

$$M' = \prod_{n=-M}^{M-1} \Delta T_n. \tag{5.4}$$

In terms of our notation, the matrix M' is given essentially by the inverse of the matrix Σ (4.11):

$$\Sigma^{-1} = \prod_{n=-M}^{M-1} U^{-1}(q_n). \tag{5.5}$$

We now rewrite the matrix $U^{-1}(q)$ in terms of a diagonal matrix,

$$U^{-1}(q) = \frac{1}{2}\begin{pmatrix}1 & 1\\ ip & -ip\end{pmatrix}\begin{pmatrix}e^{-ip\Delta x} & 0\\ 0 & e^{ip\Delta x}\end{pmatrix}\begin{pmatrix}1 & -\dfrac{i}{p}\\ 1 & \dfrac{i}{p}\end{pmatrix}, \tag{5.6}$$

so that, rearranging the products in (5.5), we can express matrix Σ^{-1} in terms of a new matrix ΔT_n,

$$\Delta T_n = \begin{pmatrix}\dfrac{p_n + p_{n+1}}{2p_n}\exp(-ip_n\Delta x) & \dfrac{p_n - p_{n+1}}{2p_n}\exp(-ip_n\Delta x)\\ \dfrac{p_n - p_{n+1}}{2p_n}\exp(ip_n\Delta x) & \dfrac{p_n + p_{n+1}}{2p_n}\exp(ip_n\Delta x)\end{pmatrix}, \tag{5.7}$$

that is exactly the matrix introduced in [22].

It is important to note that the ΔT_n matrix describes a *partition-to-partition* algorithm for KdV. Thus ΔT_n corresponds to the passage from the nth partition to the $(n+1)$th partition in the input space series.

The algorithm derived in Section 4 for NLS may instead be viewed as a *point-to-point* algorithm, which arises as a consequence of the propagator method used herein. We have seen above that the formulation given in Section 4 for NLS is equivalent to the partition-to-partition formulation of [22] for

KdV: a major advantage of the present formulation is its immediate applicability to problems in the AKNS class with *periodic boundary conditions* [45].

6. NUMERICAL RESULTS

The discrete algorithm described above has been implemented on a vector processor (FPS 500) with Fortran code. When $\sigma = -1$ the program computes the scattering coefficient $a(\zeta)$ in a chosen domain of the upper half complex plane ζ. After the discrete spectrum is determined, the program computes the continuous spectrum $\rho(\xi)$ on the real axis (3.9). If $\sigma = +1$ the program computes only the continuous spectrum. Finally the program performs some tests on the resultant spectrum using the "generalized Parseval relation" (3.14) to check if all the eigenvalues have been found.

We now consider several numerical examples in Figs. 3–8; we graph three different panels (a)–(c) to illustrate the results of each example. In the first of these panels (a) we plot the modulus of $q(x, t)$ to show the space–time evolution of the example as given by the NLS equation (computed by numerically integrating NLS, using a spectral method [29]). In the second panel (b) for each example we graph in the complex plane ζ the quantity $\ln[1 + |a(\zeta)|^{-2}]$; this allows the discrete eigenvalues to be easily recognized by their associated sharp peaks. The last of the three panels (c) gives the continuous spectrum: it shows the modulus of $\rho(\xi)$ compared with the associated modulus of the linear Fourier spectrum, which is normalized by a factor $\sqrt{2\pi}$ as in (3.20).

The first example (Fig. 3) has no continuous spectrum because the wave motion consists of a single soliton as given by (2.6). We have chosen $q_0 = -k = 1$ so that the eigenvalue is $\zeta_1 = \frac{1}{2}(1 + i)$ and $\rho_1 = -i$ [4]. The numerical results (Table I) show that the discrete eigenvalue is found to a good approximation even with a small number of discretization points, while the convergence to the coefficient ρ_1 is much slower. Fig. 3 shows the results for the 2048-point case. The Fourier spectrum (Fig. 3c) is large because it

TABLE I

Numerical Results of the Analysis of a Single Soliton Solution to NLS for Various Values of the Number of Discrete Points

Points	Δx	ζ_1 found	ρ_1 found	b_0
32	0.6250	$0.48867 + i0.47879$	$0.21506 - i0.67733$	0.03624
128	0.1563	$0.49932 + i0.49865$	$0.07191 - i0.91974$	0.00246
512	0.0390	$0.49996 + i0.49992$	$0.01915 - i0.98031$	0.00002
2048	0.0098	$0.50000 + i0.49999$	$0.00486 - i0.99511$	0.00001
Exact		$0.5 + i0.5$	$-i$	0

Note. Δx is the discretization interval; ζ_1 and ρ_1 are the coefficients of the discrete spectrum; b_0 is defined as the area under the continuous spectrum, theoretically zero in the present example.

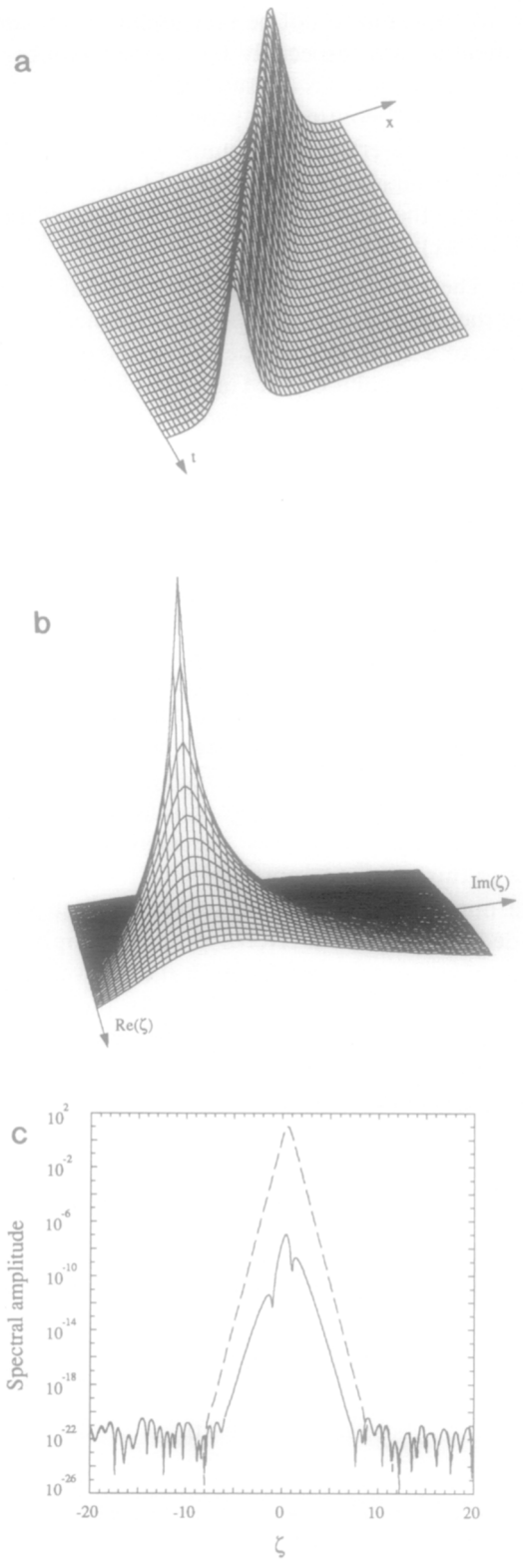

FIG. 3. One-soliton solution to the NLS equation in the focusing regime ($\sigma = -1$). Plot (a) shows the time evolution of $A(x, t)$. The spectral data in the complex plane ζ show a sharp peak associated with the soliton (b). Note the smallness of the continuous spectrum in (c) (solid line, that is theoretically zero), compared with the linear Fourier spectrum (dashed line).

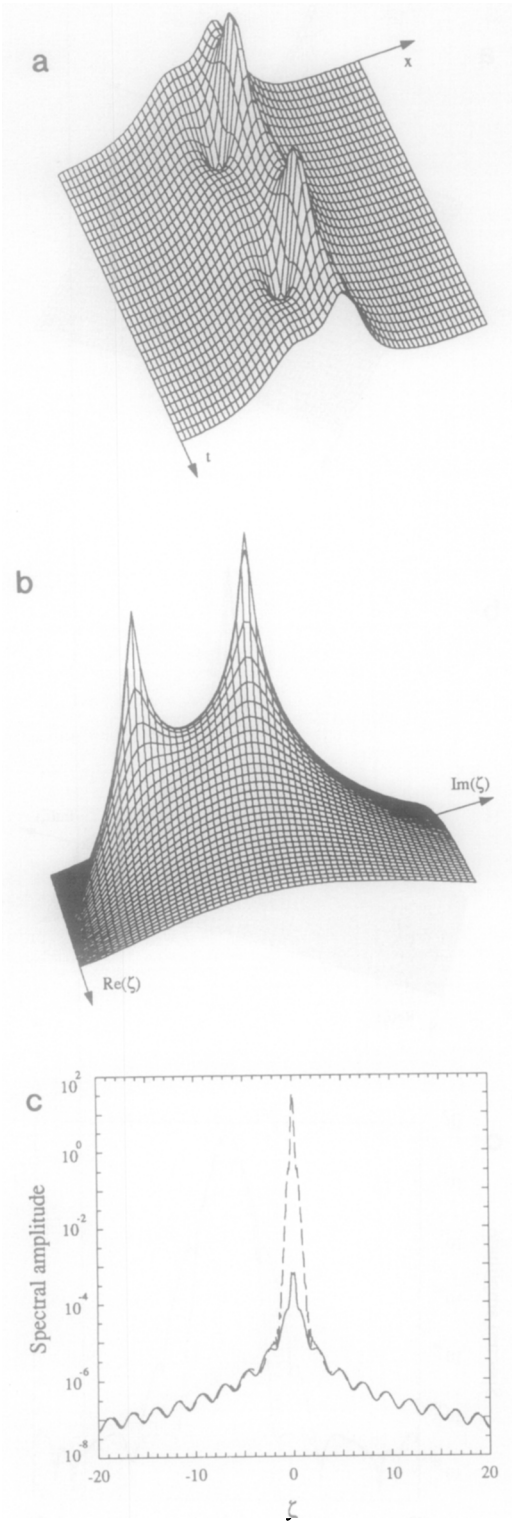

FIG. 4. A two-soliton ("breather") solution to the NLS equation in the focusing regime ($\sigma = -1$). Because the initial wave envelope $q(x, 0)$ is a real function, the two solitons do not separate in time, but instead form a periodically-evolving bound state, a "breather" (a). In (b) the discrete spectrum associated with the two soliton components of the breather. As in the previous case in Fig. 3, the continuous spectrum (solid line, theoretically zero) is many orders of magnitude smaller than the linear Fourier spectrum (dashed line) in (c).

contains the solitonic components, while the continuous spectrum is three orders of magnitude smaller; it is non-zero only because of the piecewise discretization algorithm used herein. This constitutes a noise component in algorithms of this type, which are discussed in detail elsewhere [23]; generally this small error approaches zero as $\Delta x \to 0$, as illustrated in Table I.

As a second example we have chosen a two-soliton solution to the NLS equation given by Hirota's formula [42] for 2048 points. In Fig. 4a we give the space–time evolution of two interacting solitons with amplitudes $q_1 = 1.0$ and $q_2 = 0.4$; the wavenumbers are set $k_1 = k_2 = 0$ so that the solitons have zero velocity and therefore do not separate in time (this solution is called a "breather"). In Fig. 4b we find the two eigenvalues to excellent precision and, in Fig. 4c, the continuous spectrum is seen to be quite small, five orders of magnitude lower than the linear Fourier spectrum. The non-zero continuous spectrum again results from the piecewise constant nature of the discrete algorithm employed here.

To have a theoretically non-zero continuous spectrum, we now choose an initial wave with a gaussian profile:

$$q(x, 0) = q_0 e^{-x^2}. \tag{6.1}$$

If the amplitude q_0 is small enough we find that no solitons emerge from the initial wave (in fact, one can evaluate a minimal value of the "mass" C_0 of the wave train in order to have soliton formation [4]). In Fig. 5a we choose a small value for q_0 ($=0.2$) and the initial wave is seen to disperse in time. This is confirmed by the absence of any discrete eigenvalues (Fig. 5b). The energy of the wave then lies completely in the continuous spectrum (Fig. 5c), which is very close to the linear Fourier spectrum, and the time evolution is typical of nearly linear dispersive motion.

The amplitude of the gaussian envelope is increased in Fig. 6 ($q_0 = 2.0$) and we see that the wave field now has enough mass to generate a soliton (Figs. 6a, b). The continuous spectrum (Fig. 6c) has given up some energy with respect to the Fourier spectrum in order to create the soliton. Scrutiny of Fig. 6c indicates that the energy for the soliton comes mainly from the low-wavenumber components of the spectrum.

The same gaussian initial condition evolves without generating solitons for defocusing NLS ($\sigma = +1$, Fig. 7). All the energy of the wave disperses in time, but the Fourier spectrum is no longer close to the continuous spectrum because the amplitude is no longer small.

With a higher amplitude the gaussian initial wave can generate several solitons when $\sigma = -1$. In (Fig. 8a) we can see a two-soliton breather emerging from the gaussian profile. Because the initial condition (6.1) is real, the solitons have no phase velocity, so they do not separate in time.

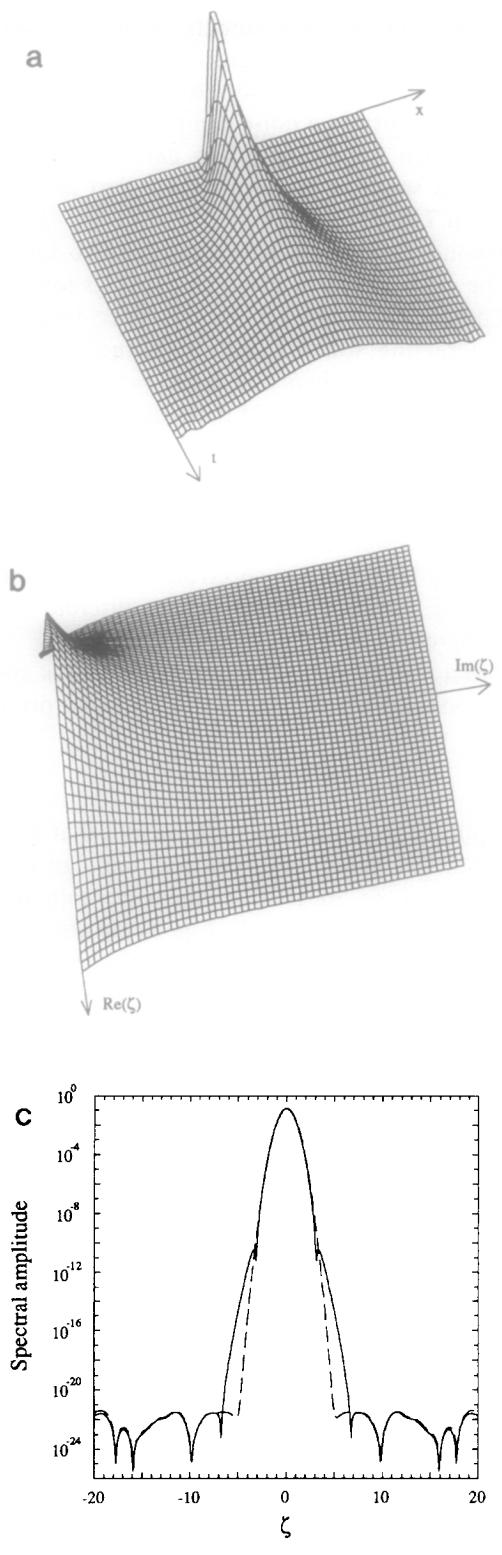

FIG. 5. Gaussian initial condition $q(x, 0)$ in the focusing regime ($\sigma = -1$). The initial wave is too small to generate a soliton (amplitude = 0.2) so that it disperses in time (a). The absence of solitons is confirmed by the absence of spectral peaks in the complex ζ plane (b). The small amplitude of the initial wave reduces the NLS equation to a quasi-linear regime, so the continuous spectrum (solid line) is close to the linear Fourier spectrum (dashed line) in (c).

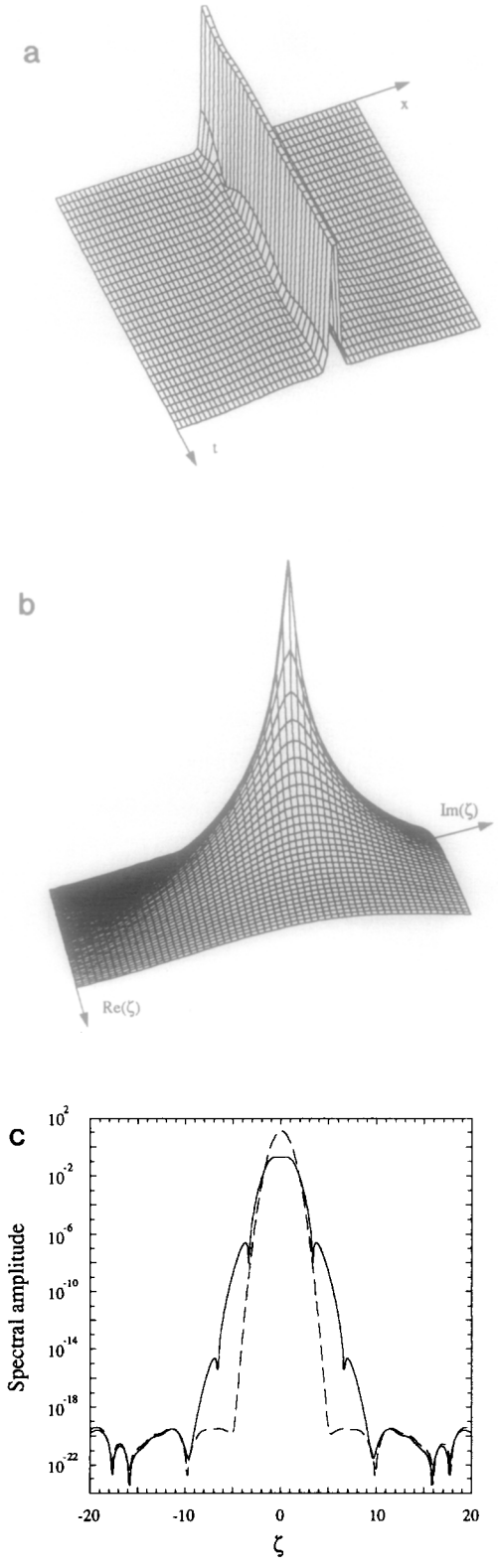

FIG. 6. The same initial condition of Fig. 5 but with a larger amplitude (the amplitude is now 2.0) in the focusing regime ($\sigma = -1$). The gaussian initial wave has enough energy to create a soliton (a) that is found by the numerical DST algorithm (b). The continuous spectrum (solid line) loses some energy at low frequency, due to the formation of the soliton, with respect to the case of Fig. 5.

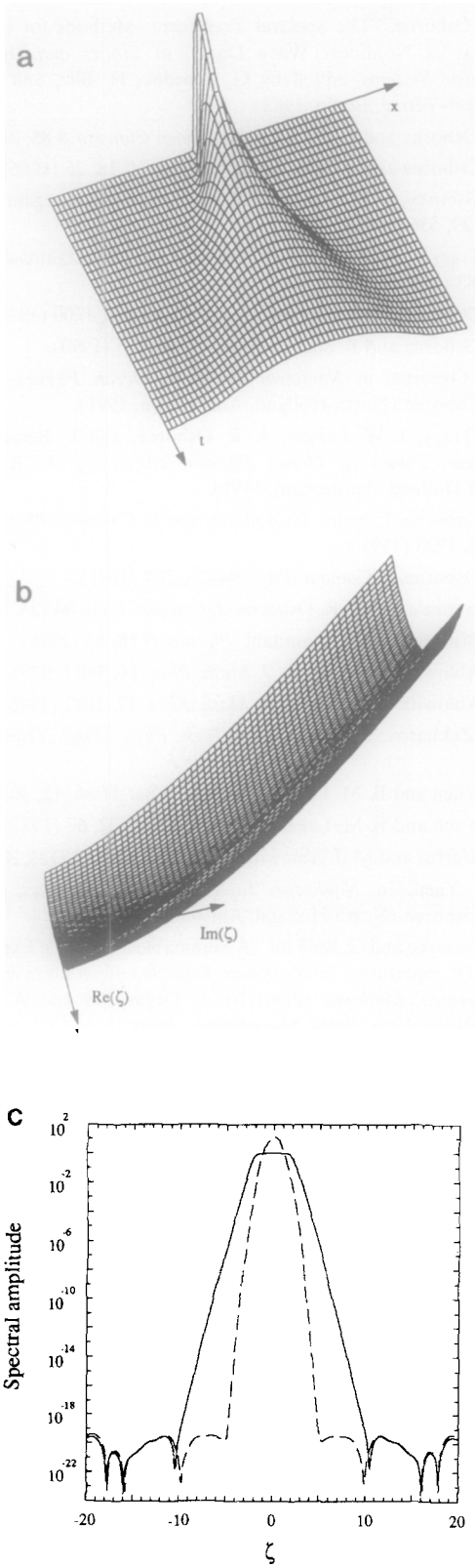

FIG. 7. Analysis of the same initial condition of Fig. 6 (amplitude = 2.0) in the defocusing regime ($\sigma = 1$). Since in this case there are no soliton solutions, the initial wave evolves dispersively (a). The spectral plane (b) contains no soliton peaks, while the continuous spectrum (solid line, (c)) is quite similar to the linear Fourier spectrum (dashed line).

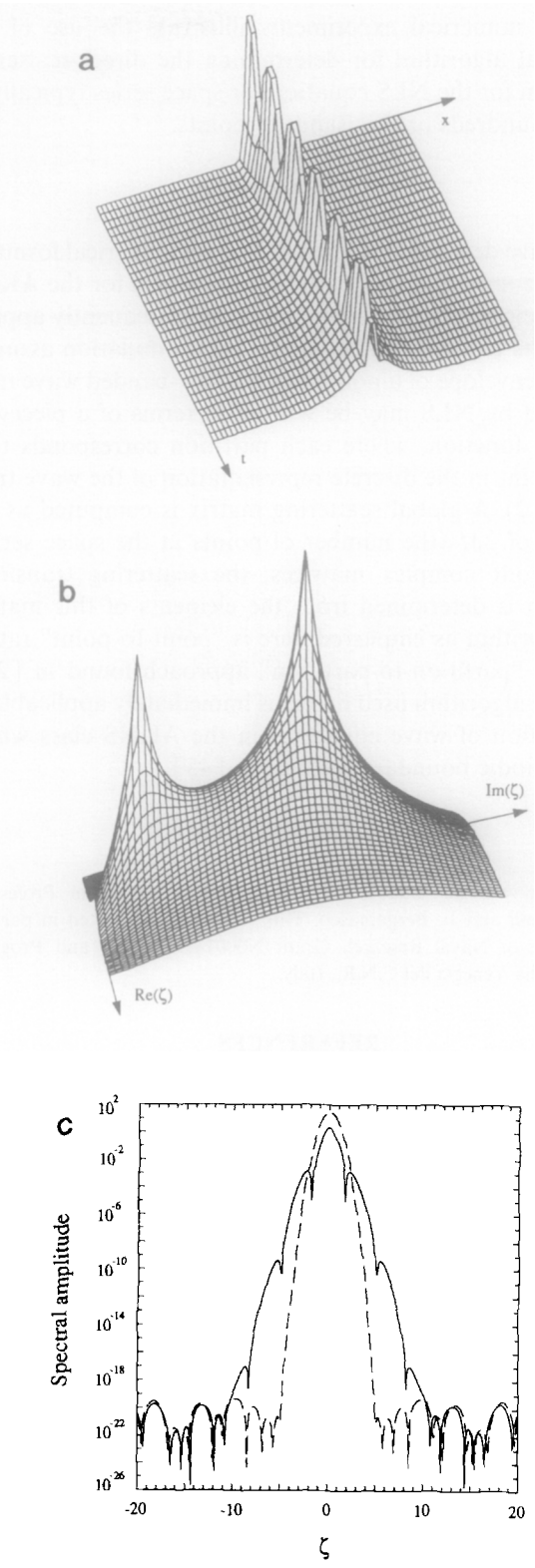

FIG. 8. Gaussian initial condition (amplitude = 3.0) in the focusing regime ($\sigma = -1$). With larger energy (compare to Fig. 6) the solution evolves into a two-soliton breather (a). The two components of the breather are found by the numerical algorithm (b). The wave is not purely solitonic because of the presence of a continuous spectrum (solid line, (c)) which is somewhat larger near the peak than the linear Fourier spectrum (dashed line).

These numerical experiments illustrate the use of the numerical algorithm for determining the direct scattering transform for the NLS equation for space series typically of several hundreds or thousands of points.

7. CONCLUSIONS

We have developed a general discrete numerical formulation for computing the scattering transform for the AKNS spectral eigenvalue problem and have subsequently applied the results to the NLS equation. The formulation assumes that the envelope of a nonlinear, narrow-banded wave train described by NLS may be written in terms of a piecewise constant function, where each partition corresponds to a single point in the discrete representation of the wave train (Figs. 1, 2). A global scattering matrix is computed as the product of $2M$ (the number of points in the space series) four-by-four complex matrices; the scattering transform spectrum is determined from the elements of this matrix. The algorithm as employed here is "point-to-point" rather than the "partition-to-partition" approach found in [22]. Thus the algorithm used herein is immediately applicable to the solution of wave equations in the AKNS class which have periodic boundary conditions [45].

ACKNOWLEDGMENTS

We acknowledge valuable aid and encouragement from Professors C. Castagnoli and L. Bergamasco. This work was supported in part by U.S. Office of Naval Research Grant N00014-92-J-1330 and Progetto Salvaguardia Venezia del C.N.R., Italy.

REFERENCES

1. C. S. Gardner, J. M. Greene, M. D. Kruskal, and R. M. Miura, *Phys. Rev. Lett.* **19**, 1095 (1967).
2. N. J. Zabusky and M. D. Kruskal, *Phys. Rev. Lett.* **15**, 240 (1965).
3. V. E. Zakharov and A. B. Shabat, *Sov. Phys. JETP* **34**, 62 (1972).
4. M. J. Ablowitz, D. J. Kaup, A. C. Newell, and H. Segur, *Stud. Appl. Math.* **53**, 249 (1974).
5. B. A. Dubrovin and S. P. Novikov, *Sov. Phys. JETP* **40**, 1058 (1974).
6. B. A. Dubrovin, V. B. Matveev, and S. P. Novikov, *Russian Math. Surv.* **31**, 59 (1976).
7. E. R. Tracy, Ph.D. thesis, University of Maryland, 1984 (unpublished).
8. Y. C. Ma and M. J. Ablowitz, *Stud Appl. Math.* **65**, 113 (1981).
9. L. A. Takhatajian and L. D. Faddeev, *Theor. Math. Phys.* **21**, 1046 (1974).
10. M. G. Forest and D. W. McLaughlin, *J. Math. Phys.* **23**, 1248 (1982).
11. A. R. Bishop, M. G. Forest, D. W. McLaughlin, and E. A. Overman II, *Physica D* **18**, 293 (1986).
12. A. R. Osborne, "The Spectral Transform: Methods for the Fourier Analysis of Nonlinear Wave Data," in *Statics and Dynamics of Nonlinear Systems*, edited by G. Benedek, H. Bilz, and R. Zeyher (Springer-Verlag, Berlin, 1983).
13. A. R. Osborne and L. Bergamasco, *Nuovo Cimento B* **85**, 2293 (1985).
14. A. R. Osborne and L. Bergamasco, *Physica D* **18**, 26 (1986).
15. A. R. Osborne, A. D. Kirwan, A. Provenzale, and L. Bergamasco, *Phys. Fluids* **29**, 656 (1986).
16. E. R. Tracy, J. W. Larson, A. R. Osborne, and L. Bergamasco, *Physica D* **32**, 83 (1988).
17. A. R. Osborne and G. Boffetta, *Phys. Fluids A* **1**, 1200 (1989).
18. A. R. Osborne and E. Segre, *Physica D* **44**, 575 (1990).
19. A. R. Osborne, in *Nonlinear Topics in Ocean Physics*, edited by A. R. Osborne (North-Holland, Amsterdam, 1991).
20. E. R. Tracy, J. W. Larson, A. R. Osborne, and L. Bergamasco, in *Nonlinear Topics in Ocean Physics*, edited by A. R. Osborne (North-Holland, Amsterdam, 1991).
21. A. R. Osborne, E. Segre, G. Boffetta, and L. Cavaleri, *Phys. Rev. Lett.* **64** (15), 1733 (1991).
22. A. R. Osborne, *J. Comput. Phys.* **94** (2), 284 (1991).
23. A. Provenzale and A. R. Osborne, *J. Comput. Phys.* **94** (2), 314 (1991).
24. A. R. Bishop and P. S. Lomdahl, *Physica D* **18**, 54 (1986).
25. M. J. Ablowitz and J. Ladik, *J. Math. Phys.* **16**, 598 (1975).
26. M. J. Ablowitz and J. Ladik, *J. Math. Phys.* **17**, 1011 (1976).
27. V. E. Zakharov, *J. Appl. Mech. Tech. Phys.* (*Engl. Transl.*) **2**, 190 (1968).
28. H. C. Yuen and B. M. Lake, *Annu. Rev. Fluid Mech.* **12**, 303 (1980).
29. H. C. Yuen and B. M. Lake, *Adv. Appl. Mech.* **22**, 67 (1982).
30. B. M. Herbst and M. J. Ablowitz, *Phys. Rev. Lett.* **62** (18), 2065 (1989).
31. H. C. Yuen, in *Nonlinear Topics in Ocean Physics*, edited by A. R. Osborne (North-Holland, Amsterdam, 1991).
32. A. R. Osborne and G. Boffetta, "A Summable Multiscale Expansion for the KdV Equation," in *Nonlinear Evolution Equations: Integrability and Spectral Methods*, edited by A. Degasperis and A. P. Fordy (Manchester Univ. Press, Manchester, 1989).
33. G. G. Stokes, *Cambridge Trans.* **8**, 441 (1847).
34. H. Hasimoto and H. Ono, *J. Phys. Soc. Jpn.* **33**, 805 (1972).
35. M. J. Ablowitz and H. Segur, *Solitons and the Inverse Scattering Transform* (SIAM, Philadelphia, 1981).
36. R. Y. Chiao, E. Garmire, and C. H. Townes, *Phys. Rev. Lett.* **13**, 479 (1964).
37. V. I. Talanov, *Sov. Phys. JETP Lett.* **2**, 141 (1965).
38. V. E. Zakharov, *Sov. Phys. JETP* **35**, 908 (1972).
39. A. Hasegawa and F. Tappert, *Appl. Phys. Lett.* **23**, 142 (1973).
40. L. Mollenauer, *Philos. Trans. R. Soc. London A* **315**, 333 (1985).
41. V. E. Zakharov and E. A. Kuznetsov, *Physica D* **18**, 455 (1986).
42. R. Hirota, *J. Math. Phys.* **14**, 805 (1973).
43. W. Mangus, *Comm. Pure Appl. Math.* **7**, 649 (1954).
44. A. R. Osborne, *J. Comput. Phys.*, submitted.
45. A. R. Osborne, in preparation, 1991 (unpublished).
46. N. N. Huang and G. Liao, *Phys. Lett. A* **154** (7–8), 373 (1991).